Improving the Performances of the Contrast Source Extended Born Inversion Method by Subspace Techniques

Krishna Agarwal, Rencheng Song, Michele D'Urso, and Xudong Chen

***Abstract*—Subspace techniques have been introduced in the framework of contrast source (CS) extended born (CSEB) model, for improving its reconstruction capabilities. Two techniques are demonstrated. First, a scheme for generating a good initial guess of the scatterer profile is shown. Second, subspace-based optimization method is used for optimization. Using the suggested techniques, CSEB model can be applied for solving inverse electromagnetic scattering problem with an extended range of application with respect to previous contributions, particularly for very high contrast lossy scatterers.**

***Index Terms*—Contrast source (CS) extended born (CSEB) model, high contrast, inverse electromagnetic scattering, strong scatterers, subspace optimization method.**

I. Introduction

THE problem of reconstructing the electromagnetic properties of the unknown objects in an inaccessible region has been of considerable research interest for a long time. In order to determine the properties of the inaccessible targets, a *nonlinear* and *ill-posed* inverse problem needs to be solved. Habashy *et al.* [1] and Caorsi and Gragnani [2] reduced the ill-posedness of the problem by first determining a minimum norm solution of the contrast source (CS). In multiresolution methods [3], [4], the problem of ill-posedness was addressed by discretizing the zoomed investigation domain at every iteration. More recently, subspace-based optimization method (SOM) [5]–[8] addressed the problem of ill-posedness by predetermining a stable portion of the CS before performing the optimization.

CS inversion (CSI) [9]–[11] indirectly worked on the nonlinearity of the problem by initiating a two-step optimization of the CS and the contrast function. In [12]–[15], linearization of the model using the Born approximation has been adopted. Instead of linearizing the model, CS extended born (CSEB) model [16]–[20] modifies the CS model of scattering without introducing any approximation such that the overall model has lesser degree of nonlinearity (DNL) (introduced in [21]) than the original model. While CSEB is suitable for inverse scattering problems involving lossy background medium, it was demonstrated in [18] that CSEB is less suitable for the problems of lossless background and lossless scatterers. It is noted that, although the applicability of CSEB to lossless problem was demonstrated with experimental data [19], [20], [22], CSEB was augmented with frequency hopping or preliminary qualitative reconstruction. Our work considers single frequency measurements and nonqualitative initial guess scheme.

We propose to introduce subspace-based techniques inspired by SOM in the framework of CSEB for extending their applicability to the problems with lossless background, lossless scatterers, and very high contrast scatterers. First, a scheme for generating an initial guess of the scatterer profile using stable portion of induced current distribution is proposed. It is well known that, for nonlinear problems, initial guess plays an important role in the convergence to the global minimum. Although Habashy *et al.* [1], Caorsi and Gragnani [2], and Chen [8] compute an initial guess for the CS, we compute an initial guess of the contrast function of the investigation domain. We show that, using the initial guess generated by the proposed scheme, CSEB can be used to reconstruct high-contrast scatterers in the lossless background as well. Second, within the framework of CSEB, it is proposed to use SOM for optimization. This is particularly useful in the reconstruction of very high contrast scatterers. Thus, if the proposed initial guess only is used in CSEB, the CSEB benefits from an initial guess of the scatterer profile (contrast function). If SOM only is used in CSEB, the CSEB benefits from the initial guess of the CS, and if both the initial guess and SOM are used, CSEB benefits from the initial guess for both the contrast function and the CS. Through these techniques, we show that the CSEB empowered with subspace techniques can be applied to many interesting and challenging cases.

Manuscript received September 11, 2011; revised January 12, 2012, March 25, 2012, and May 24, 2012; accepted May 26, 2012. This work was supported by the Ministry of Education, Singapore, under Grant R263000575112.

K. Agarwal, R. Song, and X. Chen are with the Department of Electrical and Computer Engineering, National University of Singapore, Singapore 117576 (e-mail: krishna.agarwal@nus.edu.sg; elesongr@nus.edu.sg; elechenx@nus.edu.sg).

M. D'Urso is with SELEX Sistemi Integrati, I-80014 Napoli, Italy (e-mail: mdurso@selex-si.com).

Color versions of one or more of the figures in this paper are available online at http://ieeexplore.ieee.org.

Digital Object Identifier 10.1109/LGRS.2012.2202873

II. Introduction to the CS Model

A 2-D homogeneous square region Ω is considered, which contains nonmagnetic dielectric scatterers, extending infinitely in the z-direction. The whole setting corresponds to the transverse magnetic case, where the electric fields and currents are in the longitudinal direction (z-direction) only. The permittivity at any point is given by $\varepsilon(\vec{r})$, which is equal to the background permittivity ε_b for the nonscattering locations. The region Ω is illuminated by N_s electric line sources (located at $\vec{r}_s; s = 1$ to

N_s), and the electric fields are received at N_d detectors (located at $\vec{r}_d$; $d = 1$ to N_d).

The region Ω can be discretized into M pixels of uniform shape and size such that the mth pixel is represented using $\vec{r}_m$ and the area of each pixel is a. After the discretization, the scattering formulation for all the measurements corresponding to one incidence (with source location at $\vec{r}_s$) is given as

$$\overline{E}_s^{\text{sca}} = \mathbf{G}^{\text{sca}} \cdot \overline{I}_s^{\text{ind}}, \tag{1}$$

$$\overline{I}_s^{\text{ind}} = \mathbf{\Psi} \cdot \left(\overline{E}_s^{\text{inc}} + \mathbf{G}^{\text{dom}} \cdot \overline{I}_s^{\text{ind}} \right) \tag{2}$$

where $\overline{E}_s^{\text{sca}}$ has components $E^{\text{sca}}(\vec{r}_d, \vec{r}_s)$ for $d = 1$ to N_d, $\overline{I}_s^{\text{ind}}$ is composed by $aI^{\text{ind}}(\vec{r}_m, \vec{r}_s)$ for $m = 1$ to M, and $\overline{E}_s^{\text{inc}}$ contains $E^{\text{inc}}(\vec{r}_m, \vec{r}_s)$ for $m = 1$ to M. Here, $E^{\text{sca}}(\vec{r}_d, \vec{r}_s)$ is the scattered field at $\vec{r}_d$ excited by a source at $\vec{r}_s$; $I^{\text{ind}}(\vec{r}, \vec{r}_s)$ and $E^{\text{inc}}(\vec{r}, \vec{r}_s)$ are the induced current and incident electric field at a location $\vec{r} \in \Omega$ due to the source at $\vec{r}_s$. The matrix $\mathbf{G}^{\text{sca}}$ is of dimension $(N_d \times M)$ where the (d, m)th element is $g(\vec{r}_d, \vec{r}_m)$. The matrix $\mathbf{G}^{\text{dom}}$ is of dimension $(M \times M)$ where the (m, j)th element is $g(\vec{r}_m, \vec{r}_j)$, where $g(\vec{r}', \vec{r}) = -(\omega\mu_0/4)H_0^{(1)}(k_b|\vec{r}' - \vec{r}|)$ is the Green's function corresponding to the homogeneous background medium having wavenumber k_b. The diagonal elements of $\mathbf{G}^{\text{dom}}$ are zero. The matrix $\mathbf{\Psi}$ is an M dimensional diagonal matrix, where the mth diagonal element is $a\xi(\vec{r}_m)$ and $\xi(\vec{r})$ is the scattering strength given by

$$\xi(\vec{r}) = -i\omega \left(\varepsilon(\vec{r}) - \varepsilon_b \right). \tag{3}$$

III. CSEB Model

In Section II, (2) can be written as $\overline{I}_s^{\text{ind}} = (\mathbf{I}_M - \mathbf{\Psi} \cdot \mathbf{G}^{\text{dom}})^{-1} \cdot \mathbf{\Psi} \cdot \overline{E}_s^{\text{inc}}$. As evident, the nonlinearity appears numerically from the term $\mathbf{\Psi} \cdot \mathbf{G}^{\text{dom}}$. Thus, $\|\mathbf{\Psi} \cdot \mathbf{G}^{\text{dom}}\|$ is an indicator of the DNL of the model [18]. This has been discussed in detail in [21]. For the scatterers with large contrast, the value of $\|\mathbf{\Psi} \cdot \mathbf{G}^{\text{dom}}\|$ is very large, thus indicating significant nonlinearity [17], [18]. The CSEB model [17], [18] modifies the contrast (scattering strength $\xi(\vec{r})$) using a nonlinear position-dependent function as follows:

$$p(\vec{r}) = \frac{\xi(\vec{r})}{1 - \xi(\vec{r}) f_\Omega(\vec{r})} \tag{4}$$

where $f_\Omega(\vec{r}) = \int_\Omega g(\vec{r}, \vec{r}')d\vec{r}' \approx a \sum_{j=1, j\neq m}^{M} g(\vec{r}, \vec{r}')$; $\vec{r}_j, \vec{r}_m \in \Omega$ is the tool function to change the contrast, the operator $\mathbf{G}^{\text{dom}}$, and, consequently, the nonlinearity of the whole model. Based on this modified contrast, (2) can be reformulated as

$$\overline{I}_s^{\text{ind}} = \mathbf{P} \cdot \left(\overline{E}_s^{\text{inc}} + \mathbf{G}^{\text{dom,CSEB}} \cdot \overline{I}_s^{\text{ind}} \right) \tag{5}$$

$$\mathbf{P} = a \left(\text{diag} \left([p(\vec{r}_1)\ p(\vec{r}_2)\ \cdots\ p(\vec{r}_M)] \right) \right) \tag{6}$$

$$\mathbf{G}^{\text{dom,CSEB}} = \mathbf{G}^{\text{dom}} - a^{-1}\text{diag} \times \left[f_\Omega(\vec{r}_1)\ f_\Omega(\vec{r}_2)\ \cdots\ f_\Omega(\vec{r}_M) \right]. \tag{7}$$

For this model, the DNL is measured using $\|\mathbf{P} \cdot \mathbf{G}^{\text{dom,CSEB}}\|$.

IV. Subspace-Based Techniques for Reconstruction

A. Subspace-Inspired Initial Guess of the Contrast Function

Since the operator $\mathbf{G}^{\text{sca}}$ is noninjective for extended scatterers [8], we cannot uniquely retrieve the induced currents using (1). However, a stable portion of the induced currents can be retrieved using a subspace of $\mathbf{G}^{\text{sca}}$ specified by a regularization parameter L. The induced current $\overline{I}_s^{\text{ind}}$ is split as $\overline{I}_s^{\text{ind}} = \overline{I}_s^{\text{det}} + \overline{I}_s^{\text{amb}}$, where $\overline{I}_s^{\text{det}}$ is the deterministic current and $\overline{I}_s^{\text{amb}}$ is the ambiguous current. If the left singular vectors, right singular vectors, and the singular values are denoted by $\overline{u}_l$, $\overline{v}_l$, and σ_l, then $\overline{I}_s^{\text{det}}$ and $\overline{I}_s^{\text{amb}}$ are represented as

$$\overline{I}_s^{\text{det}} = \sum_{l=1}^{L} \alpha_l \overline{v}_l\ ;\ \overline{I}_s^{\text{amb}} = \mathbf{V}^{\text{amb}} \cdot \overline{\alpha}_s^{\text{amb}} \tag{8}$$

where $\mathbf{V}^{\text{amb}} = [\overline{v}_{L+1}\ \overline{v}_{L+2}\ \ldots\ \overline{v}_M]$ and α_l, $l = 1$ to L, is computed analytically as $\alpha_l = (\overline{u}_l^* \cdot \overline{E}_s^{\text{sca}})/\sigma_l$. Setting $\overline{I}_s^{\text{amb}}$ as a null vector, an estimate of $\overline{E}_s^{\text{tot}} = (\overline{E}_s^{\text{inc}} + \mathbf{G}^{\text{dom}} \cdot \overline{I}_s^{\text{det}})$ is computed. Then, using back propagation, an initial guess of the contrast function is computed.

B. Subspace-Based Optimization Model for CSEB Model

The SOM, introduced in [8], is adapted here for the CSEB model. The computation of the deterministic current $\overline{I}_s^{\text{det}}$ has already been discussed in Section IV-A. The vector $\overline{\alpha}_s^{\text{amb}}$ [shown in (8)] contains the unknown coefficients of the vectors in $\mathbf{V}^{\text{amb}}$ and is computed using iterative optimization as described hereinafter. The cost function is defined as

$$\Delta\left(\mathbf{P}, \overline{\alpha}_s^{\text{amb}}; s = 1 \text{ to } N_s\right) = \sum_{s=1}^{N_s} \left(\frac{\left\| \overline{\Delta}_s^{\text{fie}} \right\|^2}{\left\| \overline{E}_s^{\text{sca}} \right\|^2} + \frac{\left\| \overline{\Delta}_s^{\text{sta}} \right\|^2}{\left\| \overline{I}_s^{\text{det}} \right\|^2} \right) \tag{9}$$

where $\overline{\Delta}_s^{\text{fie}} = \mathbf{G}^{\text{sca}} \cdot \overline{I}_s^{\text{det}} + \mathbf{G}^{\text{sca}} \cdot \mathbf{V}^{\text{amb}} \cdot \overline{\alpha}_s^{\text{amb}} - \overline{E}_s^{\text{sca}}$, $\overline{\Delta}_s^{\text{sta}} = \mathbf{A} \cdot \overline{\alpha}_s^{\text{amb}} - \overline{B}_s$, $\overline{B}_s = \mathbf{P} \cdot (\overline{E}_s^{\text{inc}} + \mathbf{G}^{\text{dom,CSEB}} \cdot \overline{I}_s^{\text{det}}) - \overline{I}_s^{\text{det}}$, and $\mathbf{A} = (\mathbf{I}_M - \mathbf{P} \cdot \mathbf{G}^{\text{dom,CSEB}}) \cdot \mathbf{V}^{\text{amb}}$. SOM performs the minimization of the residues in both field and state equations so that SOM is less sensitive to the choice of L. More details can be found in [6] and [23]. We use CSI-like optimization scheme similar to that in [6] and [11]. In particular, conjugate gradient is used for $\overline{\alpha}_s^{\text{amb}}$ and back propagation for $\mathbf{P}$. We make a note that, although we use the same value of L for the initial guess as well as SOM, different values of L may be used in practice.

V. Numerical Examples

We consider two algorithms for numerical experiments.

1) Algorithm with CSEB model [17], [18] and CSI-like optimization scheme [11], which shall be referred to as simply CSEB. We highlight that the optimization scheme is different from the scheme used in [18] and the

TABLE I
DESCRIPTION OF PERMITTIVITY PROFILE OF THE EXAMPLES

	Example 1	Example 2	Example 3	Example 4
Background permittivity	1	1	1	$1+i$
Permittivity of the scatterer	5	$1+4i$	$8+6i$	$8+7i$
Degree of non-linearity – CS (CSEB)	3.408 (1.008)	3.408 (0.804)	7.852 (0.9439)	5.570 (0.905)

reconstruction results may be influenced by the optimization scheme used as well. For all the simulation results presented in this letter, the cost function for CSEB is

$$\Delta\left(\mathbf{P}, \overline{\alpha}_s^{\text{amb}}; s=1 \text{ to } N_s\right) = \sum_{s=1}^{N_s} \left(\frac{\left\| \overline{\Delta}_s^{\text{fie}} \right\|^2}{\left\| \overline{E}_s^{\text{sca}} \right\|^2} + \frac{\left\| \overline{\Delta}_s^{\text{sta}} \right\|^2}{\left\| \mathbf{P} \cdot \overline{E}_s^{\text{inc}} \right\|^2} \right) \tag{10}$$

where $\mathbf{P}$ is the last updated contrast function.

2) Algorithm with CSEB model and SOM (as presented in Section IV), which shall be referred to as CSEB-SOM. For CSEB-SOM, the cost function in (9) shall be used.

If the initial guess for the contrast is computed by the method introduced in Section IV-A, the aforementioned two algorithms are referred to as CSEB(INI) and CSEB-SOM(INI), where INI refers to the proposed initial guess scheme. In addition, we consider CSEB-SOM(BG), where BG refers to the background and the initial guess of the contrast function is taken to be close to zero. We highlight that, in the previous publications on CSEB inversion methods [18]–[21], the contrast function was represented using Fourier basis. It means that the regularization was incorporated through this projection. Differently, in this letter, we consider the CSEB model alone, without Fourier basis projection. We represent the contrast function using a unit pulse function defined on each pixel as the basis. The various algorithms are compared using the same basis so that the comparison is fair.

We consider four examples to study the effect of the proposed initial guess and SOM on the reconstruction. The permittivity profiles of the scatterers and the DNL [18] are tabulated in Table I. The region Ω is of square shape of size 0.8 m. The operating frequency is 300 MHz. In each example, there is a circular scatterer of radius 0.2 m, centered at (0,0.1) m. The scatterers have high contrast as compared to various examples traditionally considered in inverse scattering problems.

It is assumed that the measurements are noisy with an SNR of 20 dB. The termination condition is $\Delta < 10^{-2}$, and the value of the regularization parameter L is chosen such that $20\log_{10}(\sigma_1/\sigma_{L+1}) > 20$ (roughly corresponding to a 20-dB SNR) [23], which corresponds to $L = 5$. The maximum number of iterations is limited to 200 for examples 1 and 2 and 500 for examples 3 and 4. Forty line sources and detectors $(N_s = N_d = 40)$ are placed uniformly over a circle of radius 2 m with its center coinciding with the center of Ω. All the forward simulations use a grid size of 64×64, and the inverse

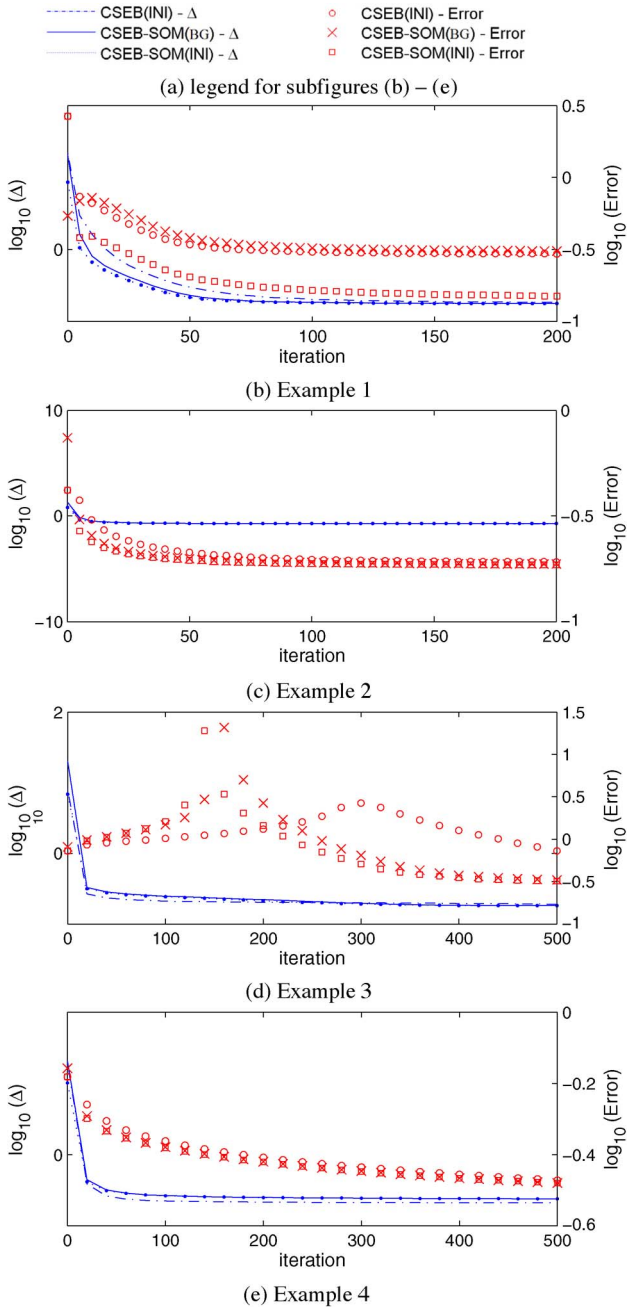

Fig. 1. Cost function and reconstruction error for all the examples with an SNR of 20 dB. The cost functions of CSEB(INI), CSEB-SOM(BG), and CSEB-SOM(INI) are quite close to each other such that they appear as overlapping.

procedures used a grid size of 32×32. In order to quantify the error in reconstruction, we use the following metric:

$$\text{Error} = \sqrt{\sum_m \left|\varepsilon^{\text{act}}(\vec{r}_m) - \varepsilon^{\text{rec}}(\vec{r}_m)\right|^2 \Big/ \sum_m \left|\varepsilon^{\text{act}}(\vec{r}_m)\right|^2} \tag{11}$$

where the superscripts "act" and "rec" denote actual and reconstructed permittivities, respectively.

The convergence curves for examples 1–4 are presented in Fig. 1(b)–(e), respectively. Both the cost function and the reconstruction error are plotted as a function of the iteration number. The reconstruction results are presented in Fig. 2 for all the four

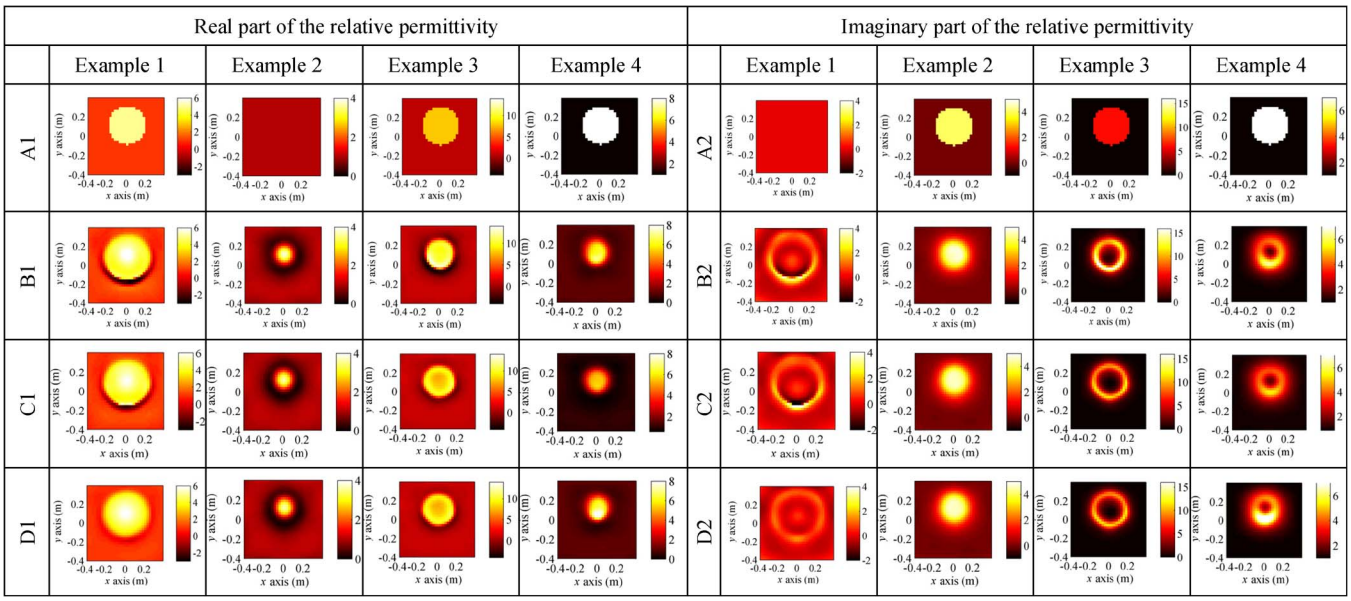

Fig. 2. Reconstruction results for all the examples for an SNR of 20 dB. (A1–D1) Real part of the relative permittivity. (A2–D2) Imaginary part of the relative permittivity. (A1 and A2) Actual values. (B1 and B2) CSEB(INI). (C1 and C2) CSEB_SOM(BG). (D1 and D2) CSEB-SOM(INI).

examples. Since examples 1–3 consider lossless background, they are difficult to reconstruct for CSEB [18]. This is verified in the convergence characteristics. However, by simply using the initial guess proposed in Section IV-A [CSEB(INI)] or using SOM for optimization [CSEB-SOM(BG)], it leads to the CSEB reconstructions to converge to true permittivity profile. Furthermore, if both the initial guess and SOM are employed [i.e., CSEB-SOM(INI)], there is an additional, although marginal, improvement in the reconstruction error.

Example 4 is interesting because, although the contrast of the scatterer is very high, the medium is somewhat lossy. CSEB(INI), CSEB-SOM(BG), and CSEB-SOM(INI) can reconstruct the scatterer with reasonable accuracy. Furthermore, from the reconstructed permittivity profiles in the last column of Fig. 2, it can be noted that CSEB(INI) and CSEB-SOM(INI) give better qualitative reconstruction than CSEB-SOM(BG), which emphasizes the importance of the initial guess.

VI. Comparison of CS and CSEB Models

It is of interest to compare the CS model with the CSEB model for high-contrast scatterers. We consider an example in which there are four scatterers, all of them with high contrast. The details of the experiment are presented in Fig. 3. We compare the CS model with CSI optimization scheme (referred to as CS), CS model with SOM (CS-SOM), CSEB, and CSEB-SOM. For a fair comparison, we use the same initial guess (computed using Section IV-A) for all the four algorithms. The convergence curves of the four algorithms are shown in Fig. 4. It is seen that, although CS and CSEB have lower values of the cost function for all the iterations [see Fig. 4(a)], the reconstruction error of CSEB and CSEB-SOM is lower than that of CS and CS-SOM [see Fig. 4(b)]. The reconstruction results are presented in Fig. 5. Although the results of these four algorithms look similar, it is still interesting to note that CS and CS-SOM provide a slightly better reconstruction of the real part of the relative permittivity, particularly for the scatterers 2

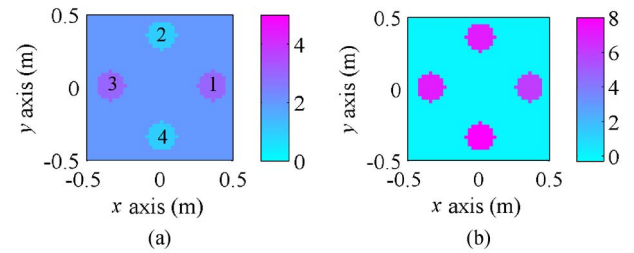

Scatterer no.	Position (m)	Relative permittivity ε_r
1	$(0.35, 0)$	$3+6i$
2	$(0, 0.35)$	$1+7i$
3	$(-0.35, 0)$	$3+7i$
4	$(0, -0.35)$	$1+8i$

- Region Ω : square of size 1 m, $\varepsilon_b = 2$.
- Frequency 400 MHz
- Forward grid size: 64×64
- Inverse grid size: 32×32
- $(N_s = N_d = 40)$
- $L = 14$
- No. of iterations = 200

(c)

Fig. 3. Example 5: Permittivity profiles of the scatterers. (a) Real (ε_r). (b) Imaginary (ε_r). (c) Details of the scatterers.

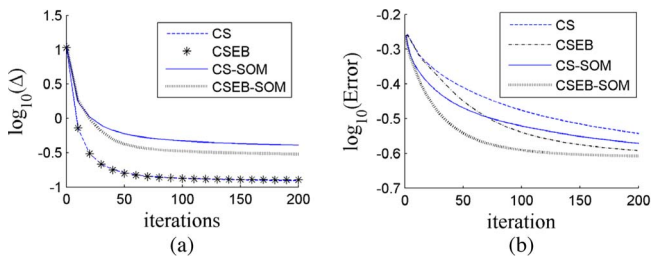

Fig. 4. Convergence characteristics of the various models (each using the initial guess proposed in Section IV-A) for example 5 (see Section VI). (a) Plot of the cost function. (b) Plot of the reconstruction error.

and 4 (with lower real part of relative permittivity than the background). However, CSEB-SOM gives the relatively best reconstruction for the imaginary part of relative permittivity of all the four scatterers and the real part of relative permittivity for scatterers 1 and 3.

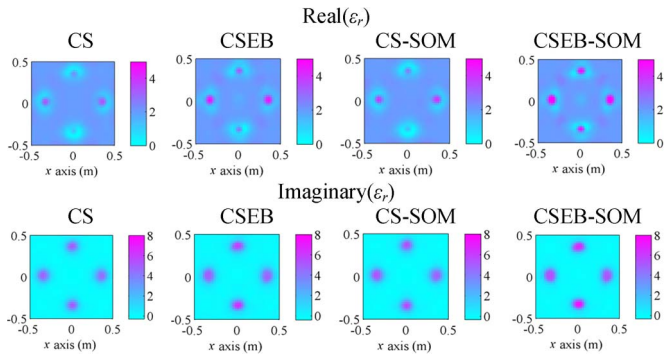

Fig. 5. Reconstruction results for the various models (each using the initial guess proposed in Section IV-A) for example 5 (see Section VI).

VII. Conclusion

In this letter, it is shown that the performances of the CSEB method can be improved using the stable portion of the induced currents in two ways, i.e., by computing a good initial guess of the contrast function and by using SOM as the optimization method. Starting from subspace techniques, the aim of this letter has been to demonstrate that the CSEB model introduced and tested in [1] and [17] can be further improved and effectively used for reconstructing very high contrast targets, embedded into lossless as well as lossy backgrounds. As a consequence, this letter successfully extends the applicability of CSEB inversion method to many interesting and challenging cases.

References

[1] T. M. Habashy, E. Y. Chow, and D. G. Dudley, "Profile inversion using the renormalized source-type integral-equation approach," *IEEE Trans. Antennas Propag.*, vol. 38, no. 5, pp. 668–682, May 1990.

[2] S. Caorsi and G. L. Gragnani, "Inverse-scattering method for dielectric objects based on the reconstruction of the nonmeasurable equivalent current density," *Radio Sci.*, vol. 34, no. 1, pp. 1–8, Jan./Feb. 1999.

[3] M. Benedetti, D. Lesselier, M. Lambert, and A. Massa, "A multi-resolution technique based on shape optimization for the reconstruction of homogeneous dielectric objects," *Inv. Probl.*, vol. 25, no. 1, pp. 015009-1–015009-26, Jan. 2009.

[4] P. Rocca, M. Donelli, G. L. Gragnani, and A. Massa, "Iterative multi-resolution retrieval of non-measurable equivalent currents for the imaging of dielectric objects," *Inv. Probl.*, vol. 25, pp. 055004-1–055004-15, May 2009.

[5] L. Pan, K. Agarwal, Y. Zhong, S. P. Yeo, and X. Chen, "Subspace-based optimization method for reconstructing extended scatterers: Transverse electric case," *J. Opt. Soc. Amer. A, Opt., Image, Sci., Vis.*, vol. 26, no. 9, pp. 1932–1937, Sep. 2009.

[6] X. Chen, "Subspace-based optimization method for solving inverse scattering problems," *IEEE Trans. Geosci. Remote Sens.*, vol. 48, no. 1, pp. 42–49, Jan. 2010.

[7] K. Agarwal, L. Pan, and C. Xudong, "Subspace-based optimization method for reconstruction of 2-D complex anisotropic dielectric objects," *IEEE Trans. Microw. Theory Tech.*, vol. 58, no. 4, pp. 1065–1074, Apr. 2010.

[8] X. Chen, "Application of signal-subspace and optimization methods in reconstructing extended scatterers," *J. Opt. Soc. Amer. A, Opt., Image, Sci., Vis.*, vol. 26, no. 4, pp. 1022–1026, Apr. 2009.

[9] A. Abubakar, P. M. van den Berg, and J. J. Mallorqui, "Imaging of biomedical data using a multiplicative regularized contrast source inversion method," *IEEE Trans. Microw. Theory Tech.*, vol. 50, no. 7, pp. 1761–1771, Jul. 2002.

[10] L. L. Li, H. Zheng, and F. Li, "Two-dimensional contrast source inversion method with phaseless data: TM case," *IEEE Trans. Geosci. Remote Sens.*, vol. 47, no. 6, pp. 1719–1736, Jun. 2009.

[11] P. M. van den Berg and R. E. Kleinman, "A contrast source inversion method," *Inv. Probl.*, vol. 13, no. 6, pp. 1607–1620, Dec. 1997.

[12] A. J. Devaney and M. L. Oristaglio, "Inversion procedure for inverse scattering within the distorted-wave Born approximation," *Phys. Rev. Lett.*, vol. 51, no. 4, pp. 237–240, Jul. 1983.

[13] S. Caorsi, G. L. Gragnani, and M. Pastorino, "Microwave imaging by 3-dimensional Born linearization of electromagnetic scattering," *Radio Sci.*, vol. 25, no. 6, pp. 1221–1229, Nov./Dec. 1990.

[14] E. L. Miller and A. S. Willsky, "A multiscale, statistically based inversion scheme for linearized inverse scattering problems," *IEEE Trans. Geosci. Remote Sens.*, vol. 34, no. 2, pp. 346–357, Mar. 1996.

[15] T. J. Cui, W. C. Chew, X. X. Yin, W. Hong, and Q. Jiang, "Super resolution phenomenon in the detection of buried objects," in *Proc. IEEE Int. Symp. Antennas Propag. Soc.*, 2003, pp. 776–779.

[16] M. D'Urso, I. Catapano, L. Crocco, and T. Isernia, "A new hybrid series expansion for 3D forward scattering problems," in *Proc. IEEE IGARSS*, Barcelona, Spain, 2007, pp. 738–741.

[17] T. Isernia, L. Crocco, and M. D'Urso, "New tools and series for forward and inverse scattering problems in lossy media," *IEEE Geosci. Remote Sens. Lett.*, vol. 1, no. 4, pp. 327–331, Oct. 2004.

[18] M. D'Urso, T. Isernia, and A. F. Morabito, "On the solution of 2-D inverse scattering problems via source-type integral equations," *IEEE Trans. Geosci. Remote Sens.*, vol. 48, no. 3, pp. 1186–1198, Mar. 2010.

[19] I. Catapano, L. Crocco, M. D. Urso, and T. Isernia, "3D microwave imaging via preliminary support reconstruction: Testing on the Fresnel 2008 database," *Inv. Probl.*, vol. 25, no. 2, pp. 024002-1–024002-23, Feb. 2009.

[20] L. Crocco, M. D'Urso, and T. Isernia, "Testing the contrast source extended Born inversion method against real data: The TM case," *Inv. Probl.*, vol. 21, no. 6, pp. S33–S50, Dec. 2005.

[21] O. M. Bucci, N. Cardace, L. Crocco, and T. Isernia, "Degree of nonlinearity and a new solution procedure in scalar two-dimensional inverse scattering problems," *J. Opt. Soc. Amer. A, Opt., Image, Sci., Vis.*, vol. 18, no. 8, pp. 1832–1843, Aug. 2001.

[22] I. Catapano, L. Crocco, M. D'Urso, and T. Isernia, "On the effect of support estimation and of a new model in 2-D inverse scattering problems," *IEEE Trans. Antennas Propag.*, vol. 55, no. 6, pp. 1895–1899, Jun. 2007.

[23] L. Pan, X. Chen, Y. Zhong, and S. P. Yeo, "Comparison among the variants of subspace-based optimization method for addressing inverse scattering problems: Transverse electric case," *J. Opt. Soc. Amer. A, Opt., Image, Sci., Vis.*, vol. 27, no. 10, pp. 2208–2215, Oct. 2010.